



Achieving a table-like magnetic entropy change across the ice point of water with tailorable temperature range in Gd-Co-based amorphous hybrids



L.Y. Ma ^a, L.H. Gan ^a, K.C. Chan ^b, D. Ding ^{a,b}, L. Xia ^{a,*}

^a Laboratory for Microstructure, Institute of Materials, Shanghai University, Shanghai, 200072, China

^b Department of Industrial and Systems Engineering, The Hong Kong Polytechnic University, Hung Hom, Hong Kong

ARTICLE INFO

Article history:

Received 28 February 2017

Received in revised form

22 June 2017

Accepted 23 June 2017

Available online 24 June 2017

Keywords:

Amorphous alloy

Hybrids

Table-like magnetic entropy change

Refrigeration capacity

ABSTRACT

Alloys exhibiting table-like magnetic entropy change ($-\Delta S_m$) profiles are regarded as ideal magnetic refrigerants for the Ericsson magnetic refrigeration cycle. In this work, we fabricated two Gd-Co-based amorphous hybrids using various combinations of $Gd_{50}Co_{50}$, $Gd_{50}Co_{48}Fe_2$, $Gd_{50}Co_{48}Mn_2$ and $Gd_{50}Co_{45}Mn_5$ amorphous ribbons with Curie temperatures ranging from 245 K to 278 K, and obtained table-like $-\Delta S_m$ profiles across the ice point of water within different temperature ranges. The maximum $-\Delta S_m$ and refrigeration capacity of the amorphous hybrids were higher than those of other amorphous alloys or composites with flattened $-\Delta S_m$ values near room temperature, indicating that amorphous hybrids are good candidates for magnetic refrigerants in house-hold magnetic refrigerators.

© 2017 Published by Elsevier B.V.

1. Introduction

The magneto-caloric effect (MCE) is the temperature change of a magnetic material under an external magnetic field. Magnetic alloys with excellent MCE can be applied as working materials in newly developed refrigeration technologies, namely, magnetic refrigeration (MR) [1–5]. MR technology has attracted increasing attention because of many advantages such as compactness, high effectiveness, low energy consumption and environmental safety over traditional gas compression technology [2–10]. As a result, magneto-caloric alloys have been intensively investigated and the number of MCE materials investigated has increased exponentially [11–22].

It is commonly accepted that a better MCE material is one that can supply the maximum amount of cooling over a widest temperature range [9–16]. Therefore, alloys undergoing a second order magnetic phase transition (SOMPT) with a substantial peak value of magnetic entropy change ($-\Delta S_m^{peak}$) seem to be ideal candidates for magnetic refrigerants due to their broadened magnetic entropy change ($-\Delta S_m$) peaks. However, for the practical application of MCE materials as magnetic refrigerants when utilizing a certain

thermodynamic cycle (e.g., the Ericsson cycle), a specific table-like profile of the MCE, where $-\Delta S_m$ is a constant with respect to temperature in the cooling region, provides optimal efficiency. Obviously, even the broadened $-\Delta S_m$ peaks of SOMPT materials are unable to match the required MCE profile, let alone the sharp but narrow $-\Delta S_m$ peaks of alloys undergoing a first order magnetic phase transition. More recently, efforts have been spent on achieving table-like magnetic entropy change around room temperature in some of the amorphous alloys or amorphous composites [11–15]. However, the maximum $-\Delta S_m$ values of these amorphous alloys or composites are not high enough for them to be used as magnetic refrigerants [12,13], and the temperature range of the table-like $-\Delta S_m$ of the single phase amorphous alloy is not tailorable [11]. Fortunately, the method used to obtain flattened $-\Delta S_m$ profile in the amorphous composite provides us with a useful way of achieving table-like $-\Delta S_m$ within a tailorable temperature range by selecting amorphous alloys with appropriate Curie temperatures (T_c) and $-\Delta S_m$ peaks [11]. According to our preliminary work, we have obtained several Gd-Co-based amorphous alloys with excellent MCE near the freezing temperature of water [17–19]. These amorphous alloys play important roles as basic alloys for fabricating the Gd-Co-based amorphous hybrids with table-like magnetic entropy change across the ice point of water within tailorable temperature ranges. In the present work,

* Corresponding author.

E-mail address: xialei@shu.edu.cn (L. Xia).

we fabricated two amorphous hybrids using a combination of $\text{Gd}_{50}\text{Co}_{50}$, $\text{Gd}_{50}\text{Co}_{48}\text{Fe}_2$, $\text{Gd}_{50}\text{Co}_{48}\text{Mn}_2$ and $\text{Gd}_{50}\text{Co}_{45}\text{Mn}_5$ amorphous ribbons with T_c ranging from 245 K to 278 K, according to a particular fraction (wt%), and obtained table-like MCE profiles near the freezing point of water, with a width of 20–40 K. The amorphous hybrids are expected to be applied as magnetic refrigerants in house-hold refrigerators.

2. Experimental methods

$\text{Gd}_{50}\text{Co}_{50}$, $\text{Gd}_{50}\text{Co}_{48}\text{Fe}_2$, $\text{Gd}_{50}\text{Co}_{48}\text{Mn}_2$ and $\text{Gd}_{50}\text{Co}_{45}\text{Mn}_5$ ingots were prepared separately by arc-melting Gd, Co, Fe and Mn elements with a purity of at least 99.9% (at%) under a titanium-gettered argon atmosphere. As-spun ribbons of each ingot were prepared under a pure argon atmosphere by a single copper wheel with a surface speed of about 30 m/s. The amorphous structures of the as-spun ribbon were checked by X-ray diffraction (XRD) on a Rigaku D\max-2550 diffractometer using $\text{Cu } K_\alpha$ radiation. $\text{Gd}_{50}\text{Co}_{50}$, $\text{Gd}_{50}\text{Co}_{48}\text{Fe}_2$, $\text{Gd}_{50}\text{Co}_{48}\text{Mn}_2$ and $\text{Gd}_{50}\text{Co}_{45}\text{Mn}_5$ amorphous ribbons with approximate dimensions 8 mm (long) \times 0.6 mm (wide) \times 40 μm (thick) were glued together according to specific fractions (wt%) for magnetic measurements. The first amorphous hybrid sample (sample 1) was fabricated by gluing together with 70% (wt%) $\text{Gd}_{50}\text{Co}_{48}\text{Fe}_2$ and 30% (wt%) $\text{Gd}_{50}\text{Co}_{48}\text{Mn}_2$ amorphous ribbons; while the second amorphous hybrid sample (sample 2) was glued together with 65% (wt%) $\text{Gd}_{50}\text{Co}_{48}\text{Fe}_2$, 25% (wt%) $\text{Gd}_{50}\text{Co}_{45}\text{Mn}_5$ and 10% (wt%) $\text{Gd}_{50}\text{Co}_{50}$ amorphous ribbons. The magnetic properties of the amorphous ribbons and the hybrid samples were measured by a Quantum Design Physical Properties Measurement System (PPMS 6000). The applied field was parallel to the longitudinal direction along the length of the sample in order to minimize the demagnetization factor.

3. Results and discussion

Fig. 1 shows the XRD patterns of the $\text{Gd}_{50}\text{Co}_{50}$, $\text{Gd}_{50}\text{Co}_{48}\text{Fe}_2$, $\text{Gd}_{50}\text{Co}_{48}\text{Mn}_2$ and $\text{Gd}_{50}\text{Co}_{45}\text{Mn}_5$ as-spun ribbons. The ribbons are predominantly amorphous without any obvious crystalline peaks on the XRD patterns. The temperature dependence of the magnetization (M - T) curves for the $\text{Gd}_{50}\text{Co}_{50}$, $\text{Gd}_{50}\text{Co}_{48}\text{Fe}_2$, $\text{Gd}_{50}\text{Co}_{48}\text{Mn}_2$ and $\text{Gd}_{50}\text{Co}_{45}\text{Mn}_5$ amorphous ribbons measured under a field of 0.03 T are shown in Fig. 2 (a). T_c values of the amorphous alloys are obtained from the derivative of their M - T curves. As marked clearly

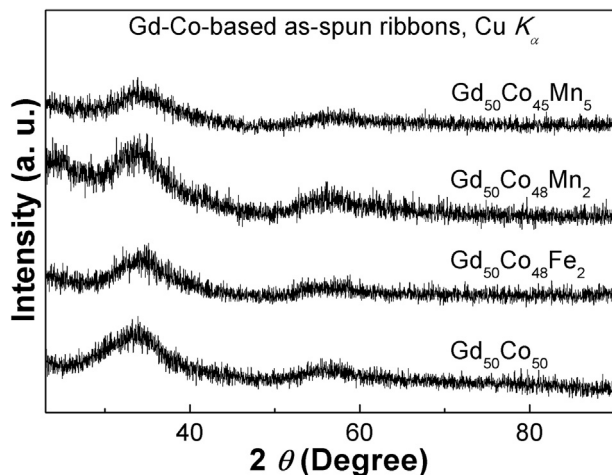


Fig. 1. XRD patterns of the $\text{Gd}_{50}\text{Co}_{50}$, $\text{Gd}_{50}\text{Co}_{48}\text{Fe}_2$, $\text{Gd}_{50}\text{Co}_{48}\text{Mn}_2$ and $\text{Gd}_{50}\text{Co}_{45}\text{Mn}_5$ as-spun ribbons obtained at a wheel surface speed of 30 m/s.

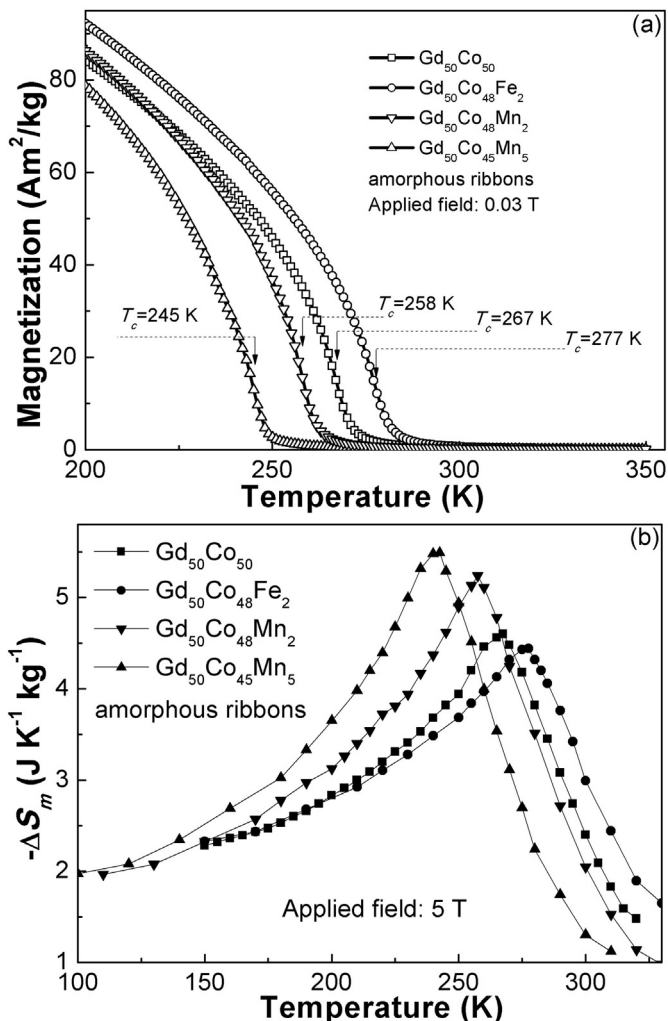


Fig. 2. (a) M - T curves of the $\text{Gd}_{50}\text{Co}_{50}$, $\text{Gd}_{50}\text{Co}_{48}\text{Fe}_2$, $\text{Gd}_{50}\text{Co}_{48}\text{Mn}_2$ and $\text{Gd}_{50}\text{Co}_{45}\text{Mn}_5$ amorphous ribbons under a field of 0.03 T, (b) the $(-\Delta S_m)$ - T curves of the amorphous ribbons under a field of 5 T.

on the M - T curves, the T_c of the $\text{Gd}_{50}\text{Co}_{50}$ amorphous alloy is enhanced to about 277 K by minor Fe addition, but decreases with Mn addition to about 258 K for the $\text{Gd}_{50}\text{Co}_{48}\text{Mn}_2$ amorphous ribbon and to about 245 K for the $\text{Gd}_{50}\text{Co}_{45}\text{Mn}_5$ amorphous ribbon. There are three kinds of exchange interactions in Gd-Co amorphous alloys: the indirect Gd-Gd, Gd-Co interactions and the direct Co-Co interaction [17–19]. The direct Co-Co interaction plays an important role in determining the T_c of the amorphous alloys, while the magnetic behavior of these alloys is mainly determined by the indirect interactions. Therefore, the improved T_c of the $\text{Gd}_{50}\text{Co}_{48}\text{Fe}_2$ amorphous alloy is closely related to the enhanced Co-Co interaction by the minor Fe addition, and the reduced Co-Co interaction in the $\text{Gd}_{50}\text{Co}_{48}\text{Mn}_2$ and $\text{Gd}_{50}\text{Co}_{45}\text{Mn}_5$ amorphous alloys leads to the decrease of T_c with Mn addition.

The temperature dependence of the magnetic entropy change $(-\Delta S_m)$ - T curves under a field of 5 T for the $\text{Gd}_{50}\text{Co}_{50}$, $\text{Gd}_{50}\text{Co}_{48}\text{Fe}_2$, $\text{Gd}_{50}\text{Co}_{48}\text{Mn}_2$ and $\text{Gd}_{50}\text{Co}_{45}\text{Mn}_5$ amorphous ribbons derived from their isothermal magnetization (M - H) curves according to the thermodynamic Maxwell equation are shown in Fig. 2 (b). The $-\Delta S_m^{\text{peak}}$ of the amorphous alloys obviously increases with the decrease of their Curie temperatures, which follows the relationship between $-\Delta S_m^{\text{peak}}$ and T_c proposed by Belo et al. from mean field theory [23].

These amorphous alloys provide ideal basic alloys for the fabrication of Gd-Co-based amorphous hybrids with table-like $-\Delta S_m$ profiles across the ice point of water within a tailorable temperature range. According to the results obtained in FeZrB(Cu) amorphous composites, the dipolar interaction between the amorphous ribbons can be neglected [12]. Therefore, the magnetic entropy change of the amorphous hybrid ($-\Delta S_m(\text{hybrid})$) fabricated by lamination of several amorphous ribbons is:

$$-\Delta S_m(\text{hybrids}) = \sum_{i=1,2,\dots,n} w_i \times (-\Delta S_m)_i \quad (1)$$

where w_i is the weight fraction of an amorphous ribbon [11–15]. We calculated $-\Delta S_m(\text{hybrid})$ of various hybrids composed of different amorphous ribbons according to various weight fractions, and found that several hybrids exhibit perfect table-like $-\Delta S_m$ profiles across the ice point of water. In this work, we employed two hybrids composed of two or three ribbons with a working temperature range of 20 K and 40 K across the ice point of water in order to ascertain the effectiveness of Equation (1).

The isothermal magnetization (M - H) curves for the hybrid sample 1 measured at temperatures ranging from 150 K to 310 K and hybrid sample 2 measured at temperatures ranging from 150 K to 320 K are shown in Fig. 3 (a) and (b), respectively. From these M - H curves, we obtained the $(-\Delta S_m)$ - T curves of the hybrid samples

according to the thermodynamic Maxwell equation, as shown in Fig. 4.

Fig. 4 (a) shows the $(-\Delta S_m)$ - T curves for the two samples under a field of 5 T. Hybrid sample 1 shows a table-like $-\Delta S_m$ within a temperature range of 20 K, while hybrid sample 2 shows a flattened $-\Delta S_m$ within a temperature range of 40 K. The maximum $-\Delta S_m$ is about $4.32 \text{ J kg}^{-1} \text{ K}^{-1}$ for hybrid sample 1 and about $4.26 \text{ J kg}^{-1} \text{ K}^{-1}$ for sample 2 under 5 T, both of which are over 12% higher than that of the amorphous $\text{Gd}_{50}\text{Co}_{45}\text{Fe}_5$ alloy [11] and over 73% higher than that of the amorphous FeZrB(Cu) composite [12]. The $(-\Delta S_m)$ - T curves for the hybrid samples under various magnetic fields are shown in Fig. 4 (b) and (c). The hybrid samples show table-like $-\Delta S_m$ profiles under various magnetic fields, indicating the validity of Equation (1) due to the negligible dipolar interaction between the different amorphous ribbons.

Another important figure of merit for the MCE materials is the refrigeration capacity [7, 11, 12, 24], which can be calculated in two ways: $RCP = -\Delta S_m^{\text{peak}} \times \Delta T_m$ (where ΔT_m is the temperature range at the half maximum of the $-\Delta S_m^{\text{peak}}$), and $RC = \int_{T_1}^{T_2} -\Delta S_m(T, H) dT$ (where T_1 and T_2 are the onset and ending temperatures of ΔT_m). As the T_1 and T_2 values of the two samples are out of the temperature range of the $(-\Delta S_m)$ - T curve measured in the present work, RCP is much larger than 691 J kg^{-1} for sample 1 and much larger than 686 J kg^{-1} for sample 2; RC is much larger than 526 J kg^{-1} for sample 1

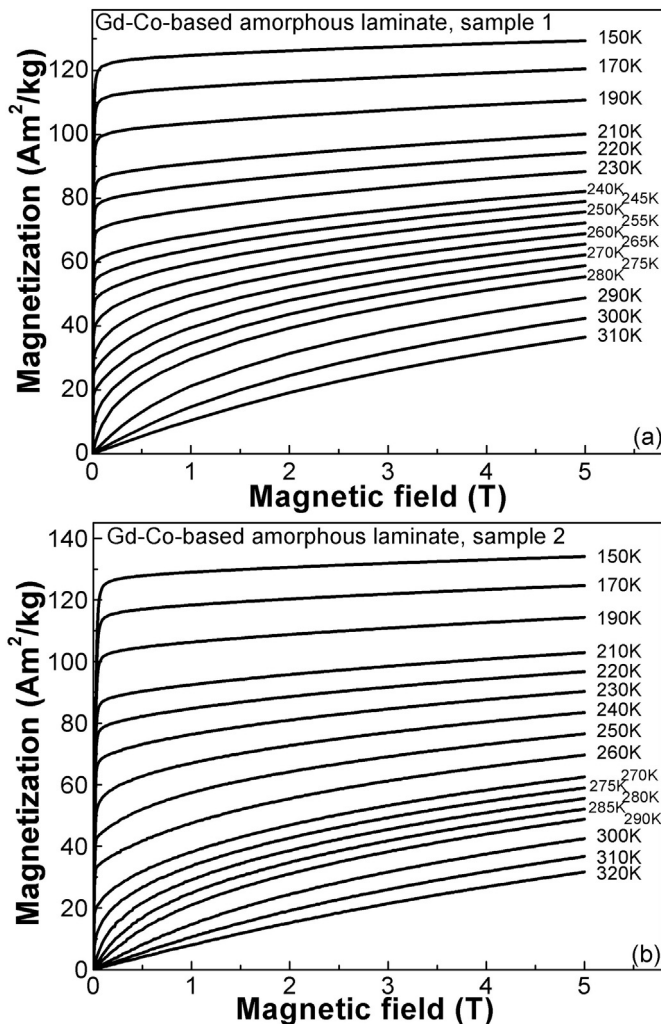


Fig. 3. M - H curves of the amorphous hybrids: (a) sample 1, and (b) sample 2.

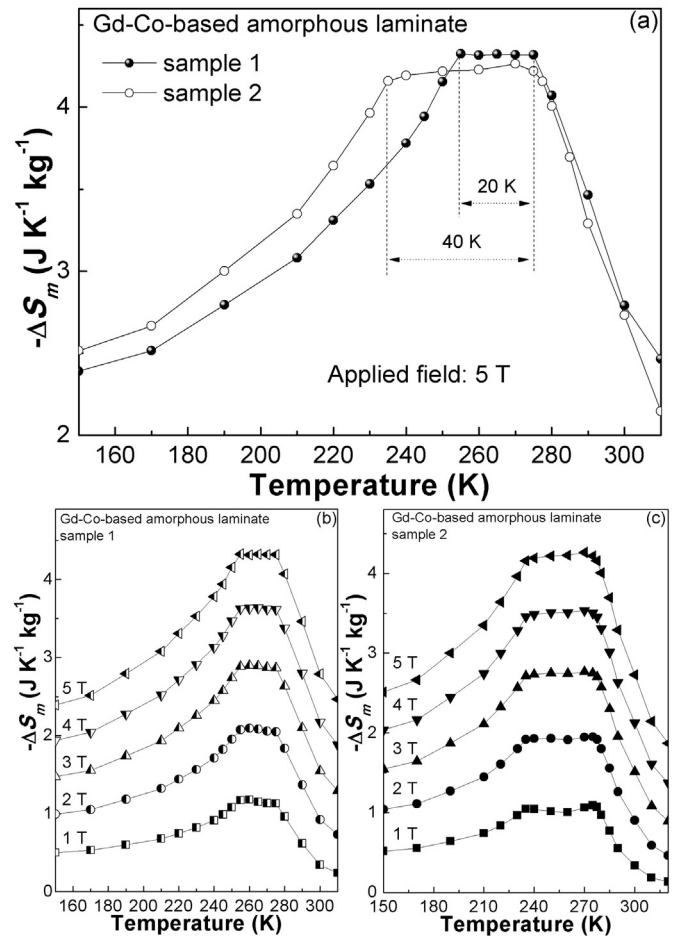


Fig. 4. (a) The table-like magnetic entropy change of amorphous hybrid samples within temperature range of about 20 K and 40 K, respectively, (b) the table-like magnetic entropy change of amorphous hybrid sample 1 under various fields, and (c) the table-like magnetic entropy change of amorphous hybrid sample 2 under various fields.

and much larger than 548 J kg^{-1} for sample 2. Both the RCP and RC values for the hybrid samples are larger than those of other materials with table-like or flattened $-\Delta S_m$ profile [11–15]. P. Álvarez et al. have recently proposed a new method to evaluate the refrigeration capacity for practical devices operating through a reversible Ericsson cycle between the cold (T_{cold}) and hot (T_{hot}) reservoirs [13]: $RC_{eff} = -\Delta S_m \times \Delta T$, where $\Delta T = T_{hot} - T_{cold}$. In case of materials showing a table-like $-\Delta S_m$ profile, ΔT is the temperature range of the table-like $-\Delta S_m$. Therefore, RC_{eff} is about 42 J/kg under 2 T and about 86 J/kg under 5 T for hybrid sample 1; about 77 J/kg under 2 T and about 166 J/kg under 5 T for hybrid sample 2. RC_{eff} of sample 1 is much higher than that of the FeZrB(Cu) amorphous composite with $\Delta T = 20 \text{ K}$, and RC_{eff} of sample 1 is also much higher than those of the FeZrB(Cu) amorphous composites with $\Delta T = 40 \text{ K}$. Considering the high maximum $-\Delta S_m$ and refrigeration capacity of the Gd-Co-based amorphous hybrids within a tailorable temperature range across the ice point of water, these hybrid samples are very promising for use as magnetic refrigerants in house-hold refrigerators.

4. Conclusions

In summary, we predicted a table-like $-\Delta S_m$ profile in several Gd-Co amorphous hybrids composed of $\text{Gd}_{50}\text{Co}_{50}$, $\text{Gd}_{50}\text{Co}_{48}\text{Fe}_2$, $\text{Gd}_{50}\text{Co}_{48}\text{Mn}_2$ and $\text{Gd}_{50}\text{Co}_{45}\text{Mn}_5$ amorphous ribbons according to Equation (1). To ascertain the validity of Equation (1), we prepared two amorphous hybrids by laminating (1) 70% (wt%) $\text{Gd}_{50}\text{Co}_{48}\text{Fe}_2$ and 30% (wt%) $\text{Gd}_{50}\text{Co}_{48}\text{Mn}_2$ amorphous ribbons, and (2) 65% (wt%) $\text{Gd}_{50}\text{Co}_{48}\text{Fe}_2$, 25% (wt%) $\text{Gd}_{50}\text{Co}_{45}\text{Mn}_5$ and 10% (wt%) $\text{Gd}_{50}\text{Co}_{50}$ amorphous ribbons. The hybrid samples exhibit table-like $-\Delta S_m$ profiles under various magnetic fields with rather high maximum $-\Delta S_m$: the maximum $-\Delta S_m$ of hybrid sample 1 under 5 T is about $4.32 \text{ J kg}^{-1}\text{K}^{-1}$, from 255 K to 275 K; while the maximum $-\Delta S_m$ of hybrid sample 2 under 5 T is about $4.26 \text{ J kg}^{-1}\text{K}^{-1}$, from 235 K to 275 K. Considering that the hybrid samples also show high refrigeration capacities and effective refrigeration capacities, these amorphous hybrid samples are very attractive for use as magnetic

refrigerants in house-hold refrigerators with a tailorable temperature range.

Acknowledgements

The work described in this paper was supported by the National Nature Science Foundation of China (Grant Nos. 51671119 and 51271103), the Research Grants Council of the Hong Kong Special Administrative Region, China (Project No. PolyU 511212).

References

- [1] E. Warburg, *Ann. Phys.* 13 (1881) 141.
- [2] O. Tegus, E. Brück, K.H.J. Buschow, F.R. de Boer, *Nature* 415 (2002) 150.
- [3] N.A. de Oliveira, P.J. von Ranke, *Phys. Rep.* 489 (2010) 89.
- [4] J. Glanz, *Science* 27 (1998) 2045.
- [5] V.K. Pecharsky, K.A. Gschneider Jr., *Phys. Rev. Lett.* 78 (1997) 4494.
- [6] E. Brück, *J. Phys. D: Appl. Phys.* 38 (2005) R381–R391.
- [7] K.A. Gschneider, V.K. Pecharsky Jr., A.O. Tsokol, *Rep. Prog. Phys.* 68 (2005) 1479.
- [8] G.V. Brown, *J. Appl. Phys.* 47 (1976) 3673.
- [9] A.M. Tishin, Y.I. Spichkin, *The Magnetocaloric Effect and its Applications*, Institute of Physics Publishing Ltd., Bristol, 2003.
- [10] B.F. Yu, Q. Gao, B. Zhang, X.Z. Meng, Z. Chen, *Inter. J. Refrig.* 26 (2003) 622.
- [11] G.L. Liu, D.Q. Zhao, H.Y. Bai, W.H. Wang, M.X. Pan, *J. Phys. D: Appl. Phys.* 49 (2016) 055004.
- [12] P. Álvarez, J.L.S. Llamazares, P. Gorria, J.A. Blanco, *Appl. Phys. Lett.* 99 (2011) 232501.
- [13] P. Álvarez, P. Gorria, J.L.S. Llamazares, J.A. Blanco, *J. Alloys Compd.* 568 (2013) 98.
- [14] H.C. Tian, X.C. Zhong, Z.W. Liu, Z.G. Zheng, J.X. Min, *Mater. Lett.* 138 (2015) 64.
- [15] J.W. Lai, Z.G. Zheng, X.C. Zhong, V. Franco, R. Montemayor, Z.W. Liu, D.C. Zeng, *J. Magn. Magn. Mater.* 390 (2015) 87.
- [16] B.J. Korte, V.K. Pecharsky, K.A. Gschneider Jr., *J. Appl. Phys.* 84 (1998) 5677.
- [17] C. Wu, D. Ding, L. Xia, K.C. Chan, *AIP Adv.* 6 (2016) 035302.
- [18] Z.W. Wang, P. Yu, Y.T. Cui, L. Xia, *J. Alloys Compd.* 658 (2016) 598.
- [19] P. Yu, N.Z. Zhang, Y.T. Cui, Z.M. Wu, L. Wen, Z.Y. Zeng, L. Xia, *J. Non-Cryst. Solids* 434 (2016) 36.
- [20] V. Franco, J.S. Blázquez, B. Ingale, A. Conde, *Annu. Rev. Mater. Res.* 42 (2012) 305.
- [21] Q. Luo, W.H. Wang, *J. Alloys Compd.* 495 (2010) 209.
- [22] L. Xia, K.C. Chan, M.B. Tang, Y.D. Dong, *J. Appl. Phys.* 115 (2014) 223904.
- [23] J.H. Bloer, J.S. Amaral, A.M. Pereira, V.S. Amaral, J.P. Araujo, *Appl. Phys. Lett.* 100 (2012) 242407.
- [24] M.E. Wood, W.H. Potter, *Cryogenics* 25 (1985) 667.